ADVANCED SENSOR RESEARCH
Open Access
www.advsensorres.com

Highly Scalable, Sensitive and Ultraflexible Graphene-Based Wearable E-Textiles Sensor for Bio-Signal Detection

*Sirui Tan, Md Rashedul Islam, Huixuan Li, Anura Fernando, Shaila Afroj, and Nazmul Karim**

Graphene-based wearable electronic textiles (e-textiles) show promise for next-generation personalized healthcare applications due to their non-invasive nature. However, the poor performance, less comfort, and higher material cost limit their wide applications. Here a simple and scalable production method of producing graphene-based electro-conductive yarn that is further embroidered to realize piezoresistive sensors is reported. The multilayer structures improved the conductivity of the piezoresistive sensors, exhibiting good sensitivity with high response and recovery speed. Additionally, the potential applications of such wearable, ultraflexible and machine-washable piezoresistive sensors as pressure and breathing sensors are demonstrated. This will be an important step toward realizing multifunctional applications of wearable e-textiles for next-generation personalized healthcare applications.

1. Introduction

Wearable electronics incorporating physical, chemical, and biological sensors and actuators have rapidly become an inseparable part of our lives for their use in a wide range of applications, especially for personalized health monitoring, wellness-tracking, and early-warning for COVID-19 and other infectious viruses.[1–3] Among them, flexible, stretchable, and miniaturized wearable sensors that measure motion, physiological, electrophysiological, and electrochemical signals emanating from the human body present great potential for personalized healthcare applications.[4–5] Such devices have received considerable attention due to their continuous and non-invasive manner.[6–7] The miniaturization of electronics, in addition to the wireless revolution, has opened up a new research era of flexible wearable electronics for remote health management of elderly personnel and children.[8] Featuring these electronics embedded into textiles, i.e., e-textiles not only presents physical flexibility,[9–10] but also allows them to interface with the human body and continuously monitor, collect, and communicate various physiological parameters.[11–12] The continuous monitoring of vital signs of the wearer, including temperature, heart rate, and oxygen saturation level, and any deviation of such vitals from their baseline can alert healthcare professionals at a very early stage and enable them to intervene more quickly.[13] Textile-based sensors also allow patients to monitor their health at home, such as self-monitoring of medical conditions with connected wearable devices could potentially reduce NHS costs by ≈60%.[14] Indeed, such a system provides a solution to the overburdened healthcare system resulting from a rapidly growing ageing society as well as maintaining and encouraging healthy and independent living for all, irrelevant of time and location.[15] Enormous efforts have been made in industry and academia to incorporate electronic components into textiles to make various forms of e-textiles.[16]

Based on various transduction mechanisms, flexible sensors could be classified as piezoelectric, capacitive, piezoresistive, and triboelectric sensors.[17–18] However, the sensitivity of the piezoelectric, triboelectric, and capacitive pressure sensors are limited due to their intrinsic disadvantages.[19] For example, the piezoelectric sensors suffer from a lack of accuracy originating from the intrinsic hysteresis and creep phenomenon of the piezoelectric materials.[20] The output signals generated from triboelectric sensors can easily be influenced by environmental conditions, such as temperature and humidity.[21] In addition to such environmental effects, capacitive sensors also suffer from nonlinearity.[22] In contrast, piezoresistive sensors have widely been

S. Tan, H. Li, A. Fernando
Department of Materials
The University of Manchester
Oxford Road, Manchester M13 9PL, UK
S. Tan
School of Textile Science and Engineering
Wuhan Textile University
Wuhan 430200, P. R. China
M. R. Islam, S. Afroj, N. Karim
Centre for Print Research (CFPR)
The University of the West of England
Frenchay, Bristol BS16 1QY, UK
E-mail: nazmul.karim@uwe.ac.uk
S. Afroj, N. Karim
The National Graphene Institute
The University of Manchester
Manchester M13 9PL, UK

The ORCID identification number(s) for the author(s) of this article can be found under https://doi.org/10.1002/adsr.202200010

DOI: 10.1002/adsr.202200010

investigated due to their simple structure, excellent sensitivity, and easy signal processing.[23] Lots of efforts have been made to improve the performance of piezoresistive sensors by developing novel materials and by designing various microstructures.[24] Nanomaterials, due to possessing high specific surface areas and unique mechanical, electronic, and thermal properties are considered promising for the improvement of sensors.[25] Among them, graphene, a single atom thick 2D closely packed honeycomb lattice of sp^2 carbon allotropes, has received much attention from the researcher community, owing to its excellent mechanical, thermal, electrical, and other properties.[26–28] Since its isolation in 2004, graphene and graphene-like 2D materials have shown great promise as transduction system and supporting substrates for fabricating next generation electronics, especially biosensors. Their extremely high surface area, coupled with a broad range of electrical and optical properties, makes them ideal for biosensing applications.[29–30] Therefore, graphene-based materials have been explored for various wearable e-textiles applications to monitor heart rate, temperature, or tracking human motion[31], which were fabricated via coating,[32] screen printing,[33] and inkjet printing[16] techniques. Embroidery is considered to be another promising technique to produce wearable e-textile components because modern embroidery machines are faster and more flexible in terms of pattern generation, also facilitating the integration of high-frequency systems into clothing.[34–35] Previous studies demonstrated the embroidery process of conductive yarns or wires to work as sensors and data conductors.[36–39] However, further work is necessary to investigate the potentiality of producing graphene-based yarns in a scalable quantity, and then integrate such electroconductive yarns into fabrics as wearable biosensors via simple embroidery technique.

Herein, we report simple and scalable embroidery of graphene-based conductive yarns to produce highly sensitive and ultraflexible, and machine washable piezoresistive sensor for biosignal detection. Graphene-based electro-conductive yarns were prepared via highly scalable and ultrafast yarn dyeing technique. Then such yarns were integrated to textiles fabrics via high-spembroidery technique to produce wearable piezoresistive sensors. The performance of such sensors was compared with the sensors made from commercially available conductive yarns. The effects of sensor structure in terms of sensor shape, design, and multiple layers were then investigated. The potential applications of such wearable e-textiles as pressure and breathing sensors were also demonstrated.

2. Results and Discussion

2.1. Scalable Production of rGO Coated Yarn

The cotton yarn was coated with reduced graphene oxide (rGO) using a laboratory-scale yarn dyeing machine. A modified Hummers method was used to prepare graphene oxide (GO), and then chemically reduced to rGO using ascorbic acid (AA) in the presence of PSS. PSS was used to functionalise the surface of rGO flakes, providing a better dispersibility and preventing agglomeration. The lateral size of GO and rGO dispersions was characterized by field emission gun scanning electron microscopy. **Figure 1**a shows the flake size distribution of the GO and rGO, which was obtained via statistical analysis of 100 flakes. The mean lateral dimension of GO and rGO was found to be ≈5.85 μm and ≈4.86 μm, respectively. The decreased flake size of GO after reduction may be due to the stresses it was subjected to during pre-mixing and centrifugation steps in post-washing cycles.[32] Figure 1b shows the flake thickness distribution of GO and rGO, which reveals that the flake thickness of GO and rGO is ≈2.07 nm and 2.2 nm, respectively. Raman spectra of GO and rGO exhibit characteristic peaks at ≈1344.78 cm^{-1} and 1605.95 cm^{-1}, corresponding to D and G bands respectively, Figure 1c. Due to the reduction, the intensity ratio of the D to G band (I_D/I_G) was increased from 0.98 for GO to 1.61 for rGO.

Figure 1d illustrates the changes in the sheet resistance of the rGO coated yarn with the coating time. The sheet resistance was found to decrease significantly with the increase of coating time. The lowest resistance was found 5 MΩ cm^{-1} after 30 min and was therefore chosen as optimized coating time to investigate the influence of the number of coating cycles on the resistance of the rGO-coated yarns. With each coating cycle, the amount of rGO flakes on the yarn surface increased, and therefore the resistance of conductive yarn decreased. This phenomenon could be explained by the absorption and adsorption phenomena. The absorption of rGO dispersion into the fibres is primarily dominant in the first few coating cycles. Once the saturation point is reached, rGO is then mainly adsorbed on the fibre surface forming a continuous conductive film by creating better connections between flakes. Thus, the sheet resistance of the yarns decreased by accumulating more rGO flakes on the fibre surface (**Figure 2**e,f) and by the restacking of the flakes through the van der Waal forces. It can be seen from Figure 1e, that the resistance of the rGO coated yarn decreased rapidly up to 5 coating cycles and afterwards, the changes in resistance were found very small. This might be caused by the saturation of the cotton yarn with rGO that is absorbing enough graphene flakes during those first 5 cycles. Figure 1f exhibits the effect of curing time and temperature on the conductivity of the rGO-coated yarn. With the increase in curing time and temperature, the residual solvents are volatilized, and the contact between the graphene flakes is increased, resulting in better conductivity of the coated yarn. The resistance was found to as minimum as 0.9 MΩ cm^{-1}. However, at higher temperatures, the strength of the cotton yarn decreases significantly. Therefore, the curing temperature of 150 °C for 3 min was chosen as the optimized curing condition for the graphene-coated yarn preparation. Scanning electron microscopy (SEM) images of silver coated thread at different magnification show that silver particles are distributed almost uniformly on the surface, Figure 2a,b. However, there are still some big particles left which might lead to uniform resistance. The silver-coated yarn was cut into small pieces of 1cm each, and then 10 samples were selected to measure the resistance of the thread. The resistance of the silver yarn was found to be 1.98 ± 0.02 Ω cm^{-1}. Figure 2c,d show SEM images of Carbon Tenax fibre, and Figure 2e,f show SEM images of graphene sewing thread at different magnifications. Compared to graphene coated yarn, carbon represents much better uniformity and smoother surface due to it being a carbon fibre twisted yarn.

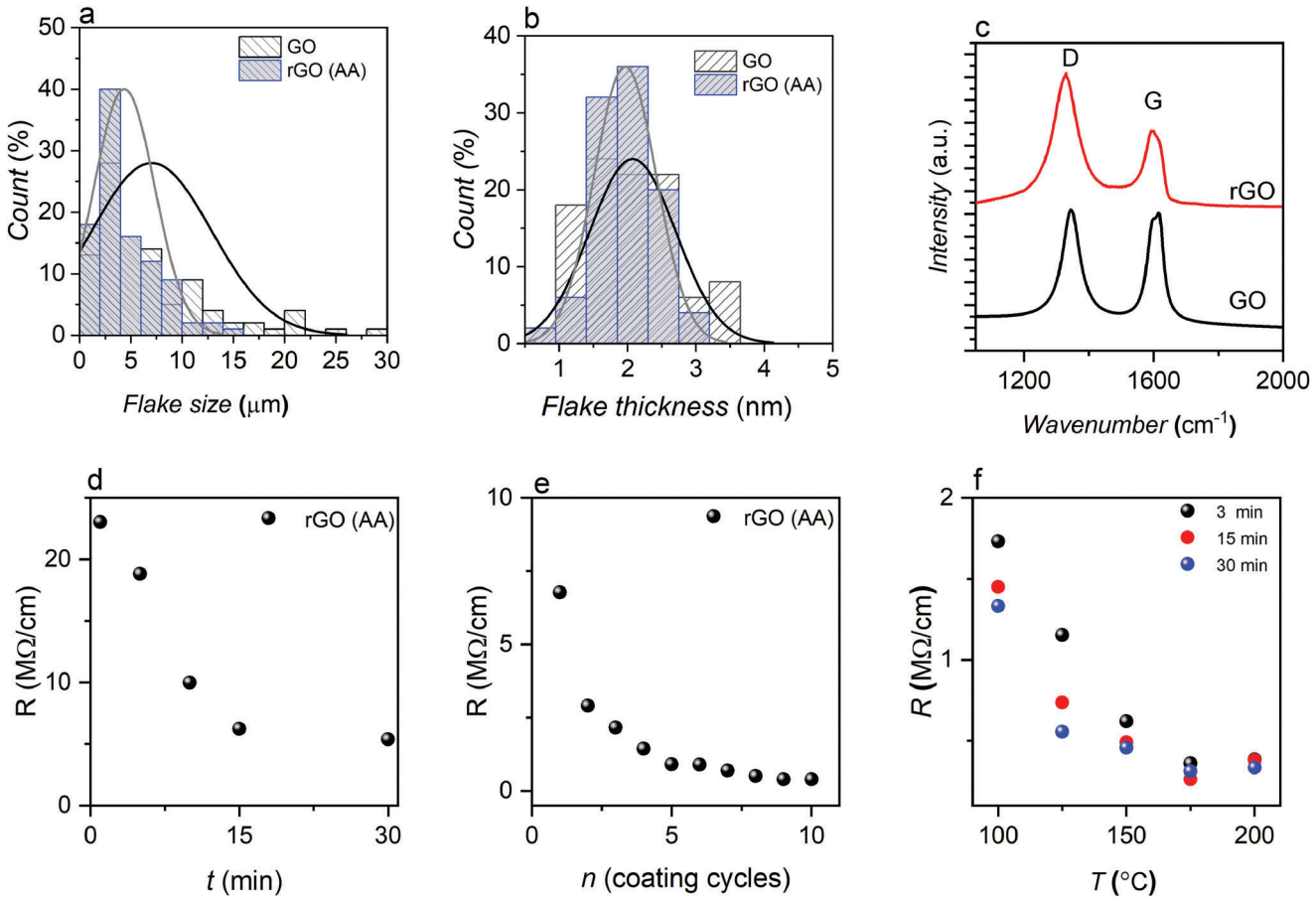

Figure 1. Preparation of rGO and rGO coated conductive yarn. a) Flake size of GO and rGO (AA) b) Flake thickness of GO anrGO (AA) c) Raman spectra of GO and rGO. d) Change of resistance of rGO yarn with coating time. e) Number of coating cycles vs resistance of rGO coated-dried yarn. f) Change of resistance of rGO yarn with curing time and temperature.

2.2. Characterization of the Conductive Sewing Thread

The investigation of three conductive sewing threads shows positive resistance variations during tensile tests and negative resistance variations during compression tests. **Figure 3**a illustrate the mechanical properties of three yarns during tensile tests. Figure 3a shows that silver-coated sewing thread provides the best elasticity among the three yarns which can be stretched to ˜10% within the elastic limit. The resistance of the thread increases rapidly during the tensile test. Carbon fibre represents a relatively higher strength but lower elasticity, which would not break until the tensile force reaches ≈52.4 N. The core of the graphene-coated thread is cotton, so the strength and the elastic limit are both relatively lower than the other synthetic yarns. Figure 3b–d represent the electrical properties of each yarn during the tensile test within the elastic limit. It is evident that, the change of resistance for graphene coated yarn were ≈4.16% (for strain upto 0.5%). The carbon yarn shows the resistance change of ≈1.38% (for strain upto 1%) and the silver yarn shows the resistance change of ≈65.24% (for strain upto 10%). However, within the same elastic limit (i.e., for the strain of 0.5%), the graphene coated yarn shows the highest change of resistance (≈4.16%), compared to both carbon (≈0.86%) and silver yarn (≈0.31%). Thus, it is evident that the graphene coated yarn shows highest sensitivity among all the yarns, as we as exhibiting linear relationship between the force and resistance. However, Figure 3e,f illustrate the compression test results of three yarns up to the breaking point and within the elastic limit. It was found that the graphene-coated thread showed a relatively better performance during the compression test, with a rapid decrease in the resistance. The silver sewing thread used in this paper is the finest yarn among these three yarns, however, their resistance only changed by 0.2 Ω cm^{-1} during the compression test from 0 to 40 pa. Compared to silver-coated threads, the carbon fibre twisted yarn shows better results, as their resistance changed by 0.2 Ω cm^{-1} during the compression test from 0–18.5 pa.

2.3. Embroidered Piezoresistive Sensor

The fabrication of the embroidered sensor involves the design of the sensor followed by an embroidery process. To investigate the effect of stitch density and stitch size on the sensor performance, for each sewing thread, 5 samples with stitch density 0.5 stitches mm^{-2} with different stitch sizes (1mm, 3mm, 5mm, 7mm, and 9mm), and 5 samples with stitch density 1 stitch mm^{-2}

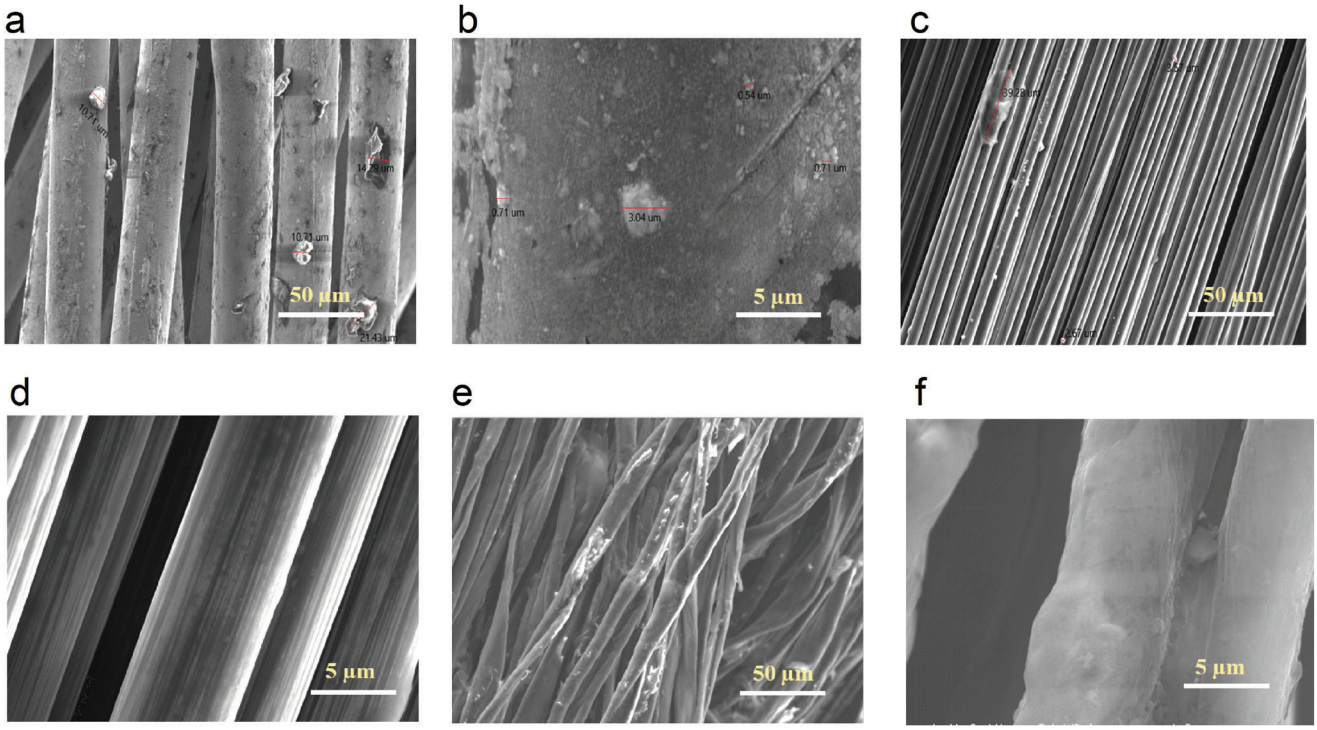

Figure 2. Characterisation of the conductive sewing yarns. SEM image of silver coated thread at a) 500X and b) 5000X magnification. SEM image of carbon Tenax at c) 500X and d) 5000X magnification. SEM image of graphene coated thread at e) 500X and f) 5000X magnification.

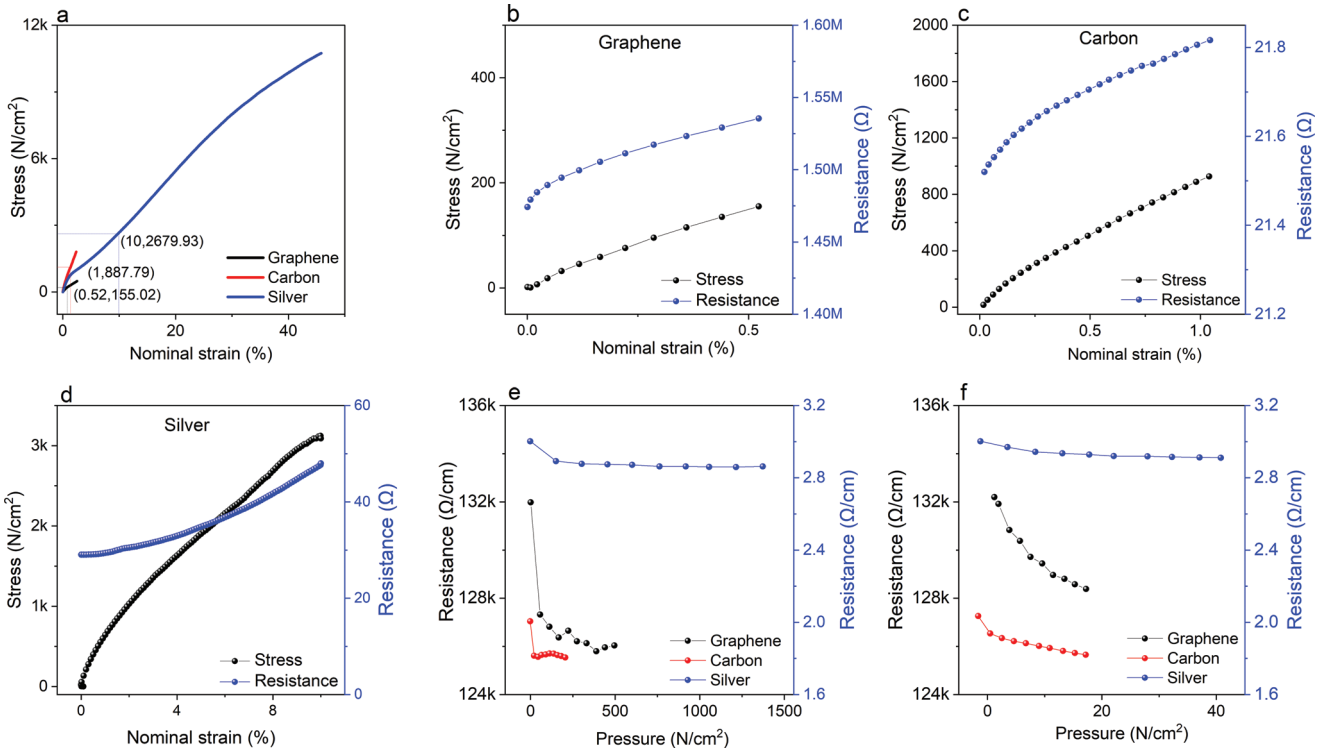

Figure 3. Mechanical properties of graphene, carbon, and silver sewing threads. a) Tensile break tests of graphene, carbon, and silver sewing threads b) Tensile tests within elastic limit of b) graphene, c) Carbon Tenax, and d) silver coated sewing thread. Yarn compression test results. Compression test of e) graphene, carbon, and silver threads up to the break point. f) Graphene, carbon, and silver threads within the elastic limit.

Table 1. The sensitivity ($\Delta R/R_0$) of the sensor with different yarns, stitch size, and stitch density.

Stitch density	Stitch size 1	Stitch size 3	Stitch size 5	Stitch size 7	Stitch size 9
Silver 0.5	−0.547%	−8.881%	−11.586%	−2.306%	−2.141%
Silver 1	−0.1883%	−3.375%	−6.042%	−10.917%	−0.605%
Carbon 0.5	−4.041%	−15.798%	−14.858%	−10.585%	−2.831%
Carbon 1	−2.766%	−10.357%	−11.926%	−9.916%	−4.829%
Graphene 0.5	−8.015%	−13.306%	−16.325%	−12.828%	−5.719%
Graphene 1	−4.580%	−10.102%	−11.687%	−15.059%	−6.103%

with different stitch size (1mm, 3mm, 5mm, 7mm, and 9mm) were prepared. The sensor size was 2 cm × 2 cm. Figure S1a (Supporting Information) is the sketch of the embroidered sensor design and Figure S1b (Supporting Information) is the carbon embroidered sensor sample with a 5 mm stitch size. The sensors were subjected to a compressive cyclic test from 0.1 to 2 N. A pre-load was applied to fix the sensor between a compression board and a wooden cube of the same size as the sensor was used to control the thrust face. The sensors were fixed and connected with the data acquisition card to record the changes in resistance. **Figure 4** represents the cyclic test results for those embroidered piezoresistive sensors.

When the stitch density increased from 0.5 to 1 sewing line per mm, the sensor with a relatively higher stitch size shows better results, especially for those sensors made with relatively thicker sewing thread (Carbon). It is evident from **Table 1**, the embroidered sensors with 5 mm stitch size performed better at 0.5 stitch density, but sensors with 7 mm stitch size performed better while the stitch density is 1. This phenomenon could be attributed to the fact that, when the stitch density increases, the sensor becomes stiffer due to the increase of the number of stitches. The same pressure was applied to the sensor, and the deformation nominal of the stiffer sensor is relatively lower than flexible sensors. As a result, the changes in resistance of the stiffer sensor is not significant as the flexible sensors. However, increasing the stitch size and stitch density at the same time can overcome this problem. Increasing stitch size makes the sensor structure looser and more flexible whereas increasing the stitch density (number of stiches in a certain area) makes the sensor tighter and stiffer. In case of a too loose and flexible sensor, e.g., 0.5 stitch density with 9 mm stitch size, when the compression pressure applied on the sensor, the conductive sewing thread might slip instead of being compressed, which might lead to a relatively lower and unstable performance. On the other hand, in case of a too tight and stiff sensor, e.g., 1 stitch density with 1 mm stitch size, the conductive sewing thread in the structure remain under a relatively higher tension, which leads to a lower deformation and lower changes in resistance during the compression test. Therefore, a series of tests were carried out (Figure 4) to find the most suitable stitch sizes for density 0.5 and 1. Table 1 is the calculated $\Delta R/R_0$ results from Figure 4. Generally, it could be assumed that for all three materials, 2 mm line separation and 5 mm stitch size for embroidered patches provides better relative changes in the electrical resistance. It is worth noting that, though the resistance of the graphene coated thread is relatively higher than carbon or silver threads, their sensitivity, namely the gauge factor is higher than that of the carbon or silver threads. Also, graphene in its reduced form interacts with the functional groups of the textiles,[32] therefore becomes an integral part of fibre facilitating a more stable funtional fibre/fabric. Instead of using rigid, toxic, nonbiodegradable, expensive, and unstable polymeric or metal substances, graphene thus offers potential for manufacturing conductive textiles for the development of next generation smart wearable e-textiles for personalized health management.

2.4. Effect of Sensor Design and Shape

To further investigate the effect of the design and shape of the embroidered sensor on the performance, five different structures were designed and manufactured (5 mm stitch size), **Figure 5**a–e. Taking into consideration the results of the yarns compression cyclic tests and sensors compression cyclic tests, carbon and graphene coated yarns were used for further experiments. The size of sensors (a) to (c) were 2 × 2 cm^2 and sensors (d) and (e) were 4 × 4 cm^2. Sensors labelled (a) to labelled (c) were conductive only single-sided due to using bottom conductive sewing thread, while sensor labelled (d) and sensor labelled (e) were conductive on both sides. The black part of the sensors was embroidered on the front side of the substrate fabric first, turned over and then the red part was embroidered on the back of the substrate. During the compression cyclic, two conductive silver fabrics (2 × 2 cm^2) were placed on the sensor (d) and (e)'s two sides to form a sandwich structure. It is evident that sensors with (d) and (e) structures represent relatively higher performance during the cyclic test. Structure (d) and (e) have a relatively higher resistance and larger changes in resistance during the cyclic tests, especially for graphene embroidered sensor. Additionally, the graphene sensor with (e) structure shows higher sensitivity than the carbon sensor. The resistance decreased approximately up to 60% from 0 to 12 500 pa, while for the carbon sensor the resistance decreased up to 45%.

2.5. Effect of Multiple Layer Structure

To compare the effect of multiple layer structure on sensor performance, embroidered sensors labelled (D) and (E) were further manufactured with 3 stitches per mm and 5 mm stitch size (**Figure 6**a) as one layer, two layers, three layers and four layers. Insulation tapes were used to fix the multiple layered structures as well as to protect the sensors. Figure 6b represents the compression test result on the tensile machine with the pressure varying from 0 to 12 500 pa (3 mm min^{-1}). The curves present almost linearity in the pressure region, especially for the sensors with two layers. The sensitivity of the sensor is a critical parameter to evaluate its performance. By increasing the layers from 1 to 4 layers, the sensitivity of the sensors was increased from −0.00278 (one layer) to −0.00505 Pa^{-1} (two layers), and then decreased to −0.00371 Pa^{-1} (three layers) and −0.00338 Pa^{-1} (four layers). It is obvious that sensors with two layers structure have a relatively higher sensitivity and linear relationship between 0 to 12500 Pa pressure. We assume thatthe electrical conductivity of the two-layered structures increases with the increase of number of layers.. Therefore, the deformation due to applied pressure corresponds to more change in the resistance of the sensors, which

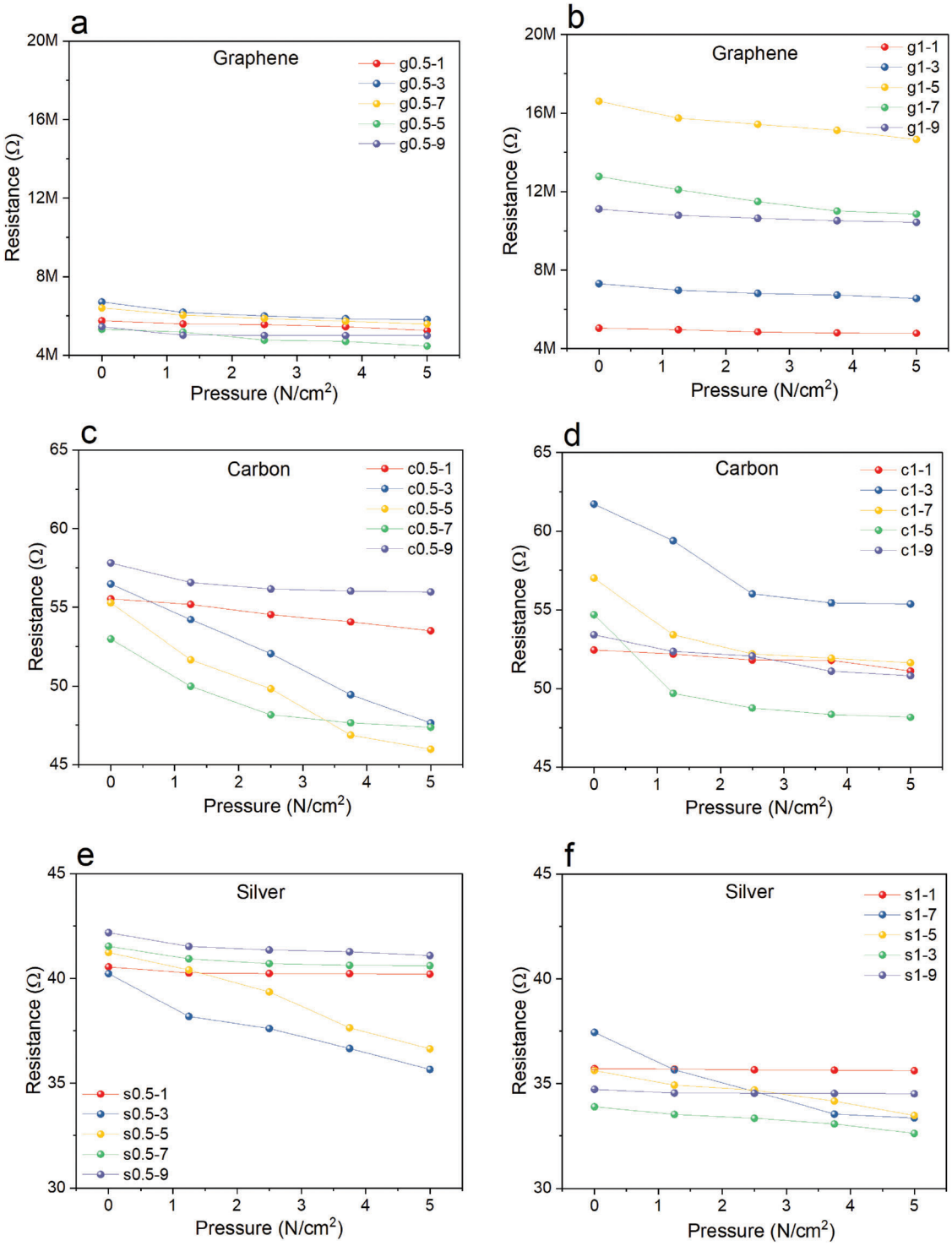

Figure 4. Compression test results of a,b) graphene, c,d) carbon, and e,f) silver piezoresistive sensor.

increased the sensitivity of our piezoresistive sensor. On the other hand, for the three and four- layered sensors, as the thickness increases, the flexibility of the sensors is decreased, and they become more rigid. Thus, the corresponding change in the resistance due to applied pressure is not significant,which reduces the sensitivity of the sensors. As a result, the sensitivity of the four-layered sensor was found to less than the three-layered sensor. To test the durability and stability of the best sensitive i.e., two layered sensor, a 400 cycles cyclic test and a long-term stability test were further employed, Figure 6c,d. During the cyclic

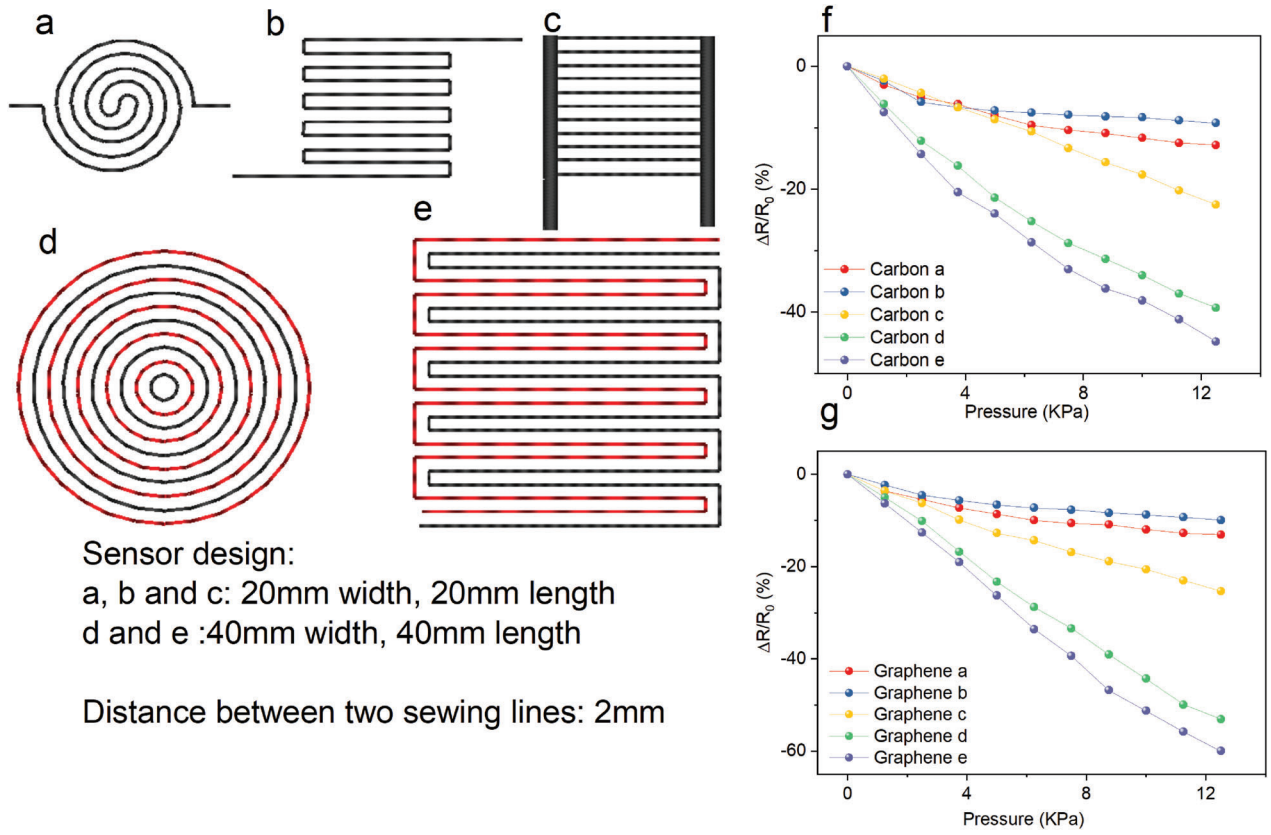

Figure 5. Design and shapes of a–e) five different sensors, cyclic compression test results of f) carbon and g) graphene Sensors.

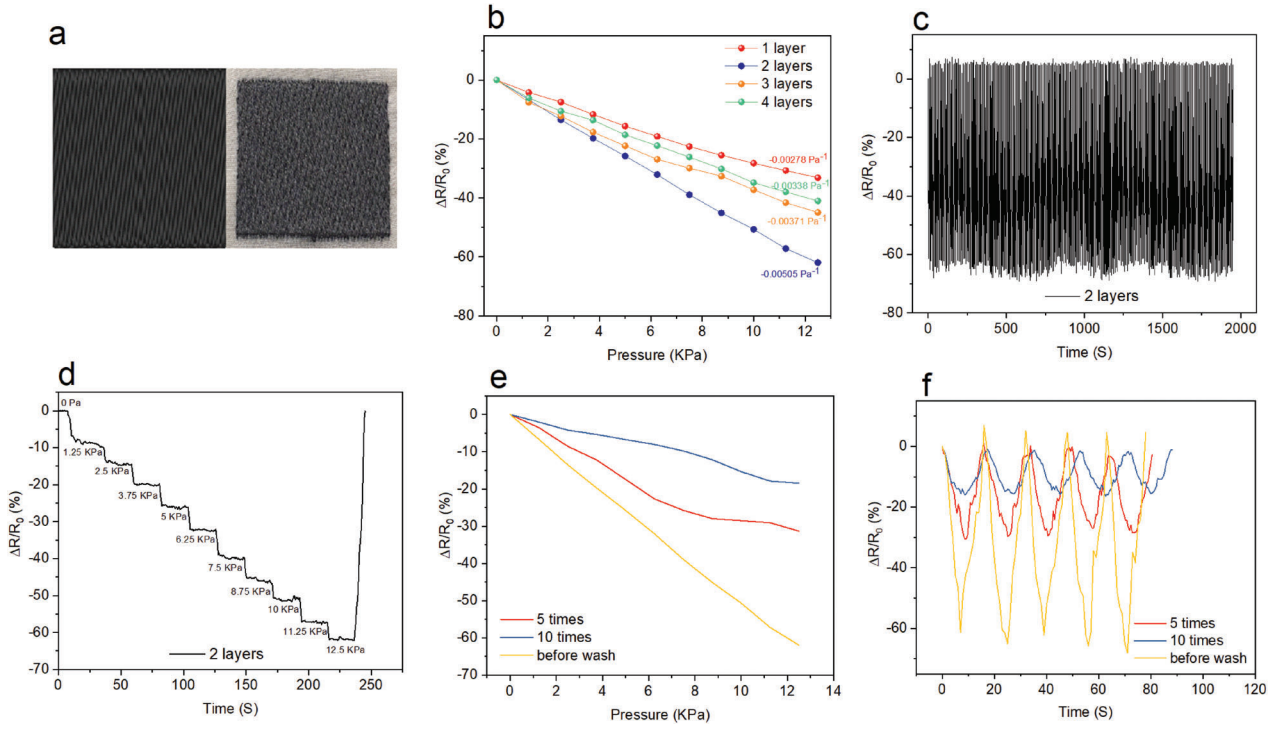

Figure 6. Effect of multiple layer structure and washability tests of embroidered sensors. a) Sketch of the design (left) and prototype of the sensor (right) b) Compression test result of sensors with different layers c) Cyclic test result of the two layers sensor, d) long-term stability test result of the 2 layers sensor e) compression test of the 2 layers sensor before and after wash, f) cyclic test result of the 2 layers sensor before and after wash.

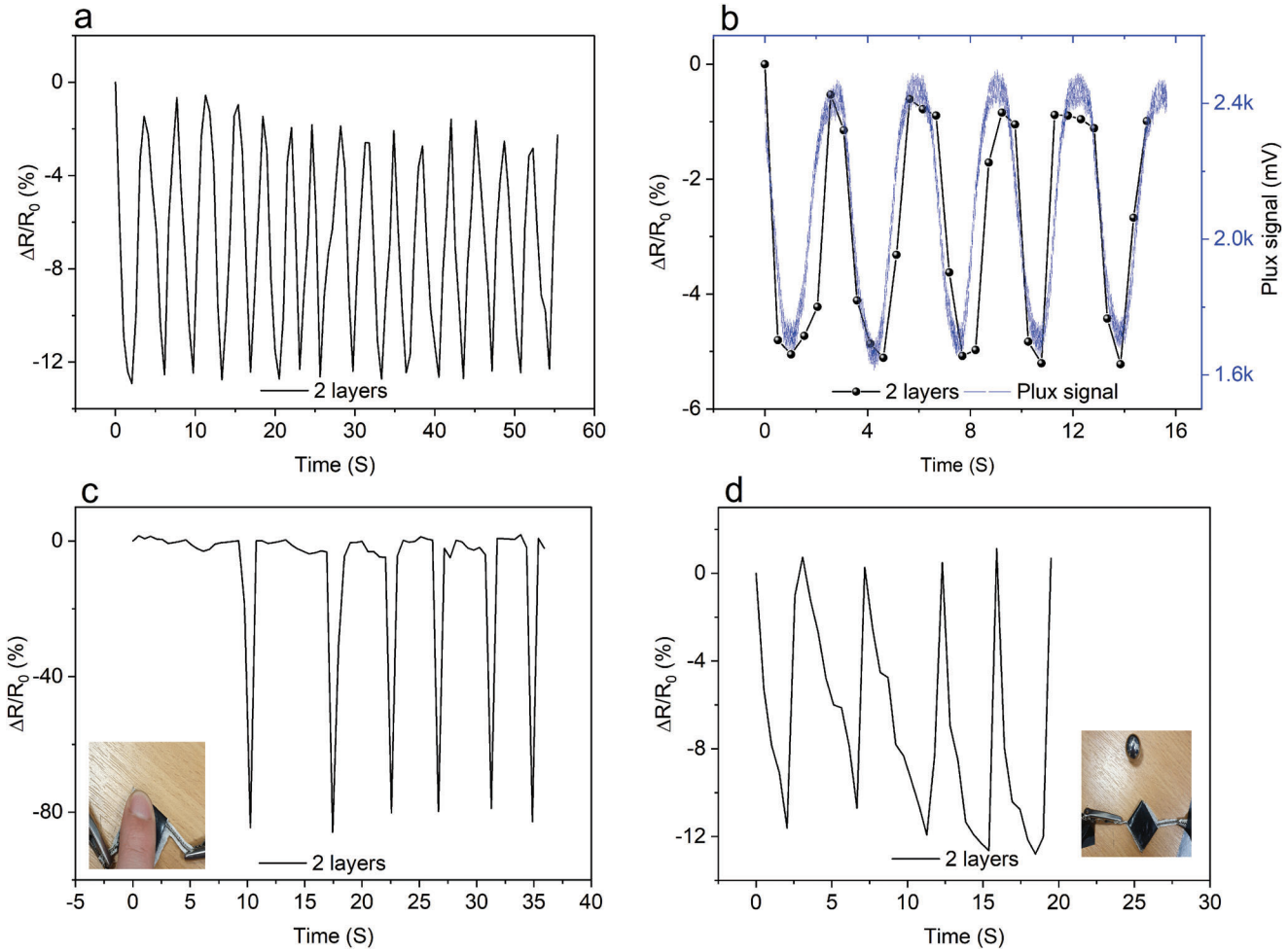

Figure 7. Application of the 2 layered embroidered sensor for a) breath test, b) breath test with the Plux signal system, c) finger touch test, and d) ball hit impact test.

test, the sensor exhibited a good stability and durability, and the resistance of the sensor was not changed significantly after the test. Additionally, the sensor showed good retention and stability since there was no significant variation of the resistance while the applied pressure was stable at different values.

2.6. Bio-Signal Detection of the Piezoresistive Sensor

To investigate the bio-signal sensing performance of our piezoresistive sensors in real-life implications, optimized two-layered sensors were further tested as a breathing sensor, **Figure 7**a. The Plux system was used as the control test, the two-layered sensors were placed under the Plux elastic band around the chest location, Figure S2 (Supporting Information). The NI-9219 card was connected with the sensor to record the changes in the resistance during the breath test. Figure 7b illustrates the performance of the sensors, the curve of the two-layered sensor is almost identical to the Plux sensor, which indicates the prospect of our sensor as a bio signal detection tool. Figure 7c,d exhibits the changes in the relative resistance during the finger touch test and the ball hit impact test, respectively. In both cases, it is seen that these two-layered piezoresistive sensor has a good response speed and recovery speed making the sensor capable of functioning as a wearable sensor for human movement detection and bio-signal detection.

2.7. Washability of the Embroidered Sensor

Washability is an essential property of wearable sensors. The washability test of our piezoresistive sensors was conducted following the BS EN ISO 105 C06 A1M test method. The resistances of the sensors were measured after 5 and 10 washing cycles. After drying, a single compression test and a 5 cycles cyclic test were carried out, Figure 6e,f. It is evident that washed sensors exhibited relatively poor performance than the unwashed sensors. The total resistance increased by 17.6% after 5 times washing and 42.3% after 10 times washing. During the washing process, the vessel containing the rGO coated cotton yarns was shaken, and the oscillation of the washing bath simulated the stress generated during the standard washing cycles, which might affect the integrity and continuity of the deposited layer, increasing the sheet resistance.[40] The wash tests have a big influence on the

signal output stability, sensitivity and conductivity of the sensor. However, the wash stability of wearable e-textiles can be improved via several methods,[41] such as pre- or post-treatment with substances that can act as a molecular glue, polyurethane (PU) sealing, or hot melt encapsulation, etc.[42] without changing the mechanical and electrical properties of the wearable sensors.

3. Conclusion

In this study, we report a simple and scalable production method for rGO dispersion and the coating of cotton yarns with the rGO dispersion to produce electrically conductive graphene coated yarn. The graphene-based electroconductive yarns thus produced are comparable with the commercially available conductive yarns. The yarns show excellent sensitivity and cyclability when embroidered into a piezoresistive sensor. We also found that multilayer structures could potentially improve the conductivity of the piezoresistive sensors; especially the modified two-layered embroidered sensor show good sensitivity with high response and recovery speed. In addition to working as a pressure sensor, our piezoresistive sensor performed as a breathing sensor, which was comparable with the commercial sensors. Although the washability of the sample is not satisfactory, it could be improved by pre- or post-treatment with encapsulation materials. We believe our simple production method of graphene-based wearable sensors would be an important step toward realizing multifunctional applications of wearable e-textiles for next generation health care devices.

4. Experimental Section

Materials: Flake graphite grade 3061 was kindly supplied by Asbury Graphite Mills, USA. L-ascorbic acid (≈99%), ammonia, and poly (sodium 4-styrene sulfonate) (PSS, Mw ≈70 000, powder) were purchased from Sigma-Aldrich, UK, and used as received. Surface-pre-treated (scoured and bleached) 100% cotton yarn from the University of Manchester textiles laboratory was used. To investigate the performance of graphene-coated yarn with the commercial yarns, metal-coated and non-metallic conductive yarns were chosen as the control yarns. Silver-coated polyamide yarn (Silverpam 250) and carbon yarn (Carbon Tenax) were purchased from TIBTECH innovations, France. The nonconductive polyester sewing thread (ISACORD 40) was purchased from Barnyarns Ripon Ltd, UK. Woven cotton substrate fabric was manufactured internally in the University of Manchester weaving laboratory and water-soluble PVA backing materials were purchased from Abakhan Fabrics, Hobby & Home, Manchester, UK.

Synthesis of Graphene Materials: Graphene oxide (GO) was prepared using a modified Hummers method.[43] A brown dispersion of GO (1 mg mL^{-1}) was prepared by adding 160 mg of GO to 160 mL of deionized (DI) water and sonicated for 30 min. In order to form a stable dispersion, 1.6 g of PSS was mixed into the GO dispersion by vigorous stirring. The resulting suspension was transferred to a round-bottom flask placed in an oil bath. Ascorbic acid (1.2 g) and NH_3 (required to adjust pH 9–10) were added to the dispersion with vigorous stirring. This mixture was held at 90 °C for 72 h under closed conditions to obtain a black dispersion. Residual ascorbic acid and PSS were removed from the rGO by washing several times with deionized water and finally diluted into distilled water (DI) to adjust the rGO dispersion concentration to 3.2 mg mL^{-1}.

Coating of Textile Yarn with Graphene-Based Ink: A simple dip-coating method was used to coat the cotton textile yarn with the graphene-based ink. Coating and curing conditions such as coating time, the number of coating cycles, curing time, and temperature were optimized. First, a scoured–bleached cotton yarn was coated with the rGO dispersion (≈1.9 mg mL^{-1}) for 1–30 min. Then resistance per cm length of the coated yarn was measured using a multi-meter (DL9309 Auto Ranging multi-meter, Di-Log, UK). The optimized coating time was used to coat yarn with the same rGO dispersion for a number of coating cycles (up to 10). The changes in the electrical resistance after each cycle were observed and optimized for further studies. The effects of the curing time (5–30 min) and the curing temperature (100–200 °C) on the resistance of the rGO-coated yarn were then observed and optimized. Then a laboratory-scale yarn dyeing machine was used to produce a batch of rGO-coated textiles yarns in scalable quantity.

Characterization of the Conductive Sewing Thread: To investigate the capability of our graphene-coated yarn to manufacture the textile sensors, commercially available silver-coated metallic yarn and non-metallic carbon-conductive yarns were chosen as control samples. Silver was selected due to its high conductivity. The silver sewing thread used in this study is a grafted antibacterial silver-coated thread with a resistance of 198 Ω m^{-1}. The thread also exhibits a stretchability of up to 10% that is an ideal material for sensor construction. However, the oxidisation is not avoidable even with an antibacterial layer. Carbon materials are usually strong, stable, and relatively cheaper. Carbon Tenax, used in this study, is a carbon fibre Z twisted sewing thread with a resistivity of 218 Ω m^{-1}. Although the easily broken property of the carbon fibre is unavoidable, their higher conductivity and excellent washability are much better than carbon-coated materials. The surface morphology of three conductive sewing threads was characterized by the Hitachi 3000 scanning electron microscope. Tensile and compression tests were carried out for the characterization of the conductive sewing thread using a Zwick/Roll computerized tensile testing machine (Germany). A National Instrument data acquisition card (NI-9219) was used to record the changes in resistance during the tests.

Embroidered Piezoresistive Sensor: The embroidered sensor consists of conductive lower sewing thread, nonconductive upper sewing thread, substrate fabric, and backing material. To produce embroidered piezoresistive sensors, the sensor pattern was designed on PE-Design software. The stitch density and stitch length were selected through the modelling work, and the yarn tension was adjusted in the embroidered machine to control the ratio between the upper thread and the lower thread. In this study, the sensor stitch size was altered between 1, 3, 5, 7, and 9 mm and the stitch densities were altered from 0.5 or 1 sewing line per mm. The upper thread was usually nonconductive yarn to prevent the conductive particles from the friction between the upper thread and the needle hole. The piezoresistive sensor's sensitivity (S) is an essential parameter for assessing device performance and was characterized using the following equation:

$$S = \frac{\Delta R}{R_0} = \frac{R - R_0}{R_0} \times 100 \quad (1)$$

where ΔR denote the resistance change before and after load applied, R and R_0 denotes the loaded and unloaded samples' resistances, respectively.

The embroidered piezoresistive sensors were subjected to a compressive cyclic test starting from 0.1 to 2 N using a computerised Zwick/Roell tensile tester machine. The ramp and release rates were set at 3 mm min^{-1}. The electrical response was continuously monitored and recorded using a National Instrument-9219 data acquisition card. To test the long-term stability, the piezoresistive sensor was compressed and released for 100 cycles using the tensile tester machine. A plux system was used to measure the BCG signals from a human body without a direct skin contact following appropiate risk assessment, and censent from the participant.

Washability Tests of the Piezoresistive Sensor: The washability of the rGO-coated embroidered sensors was assessed according to BS EN ISO 105 C06 A1M, by treating rGO-coated yarns in a solution containing 4 g L^{-1} ECE reference detergent B with 10 stainless steel balls at 40 °C for 45 min. A Roaches Washtec-P TOC 3002 was used for the washability test. The steel balls were used to simulate the agitation and abrasion that a garment was subjected to during a standard washing cycle. The sensors were rinsed subsequently in running water at ambient temperature and air-dried at

room temperature prior to further analysis. The sensors were tested after 5 and 10-times washing cycles.

Supporting Information

Supporting Information is available from the Wiley Online Library or from the author.

Acknowledgements

Authors gratefully acknowledge funding from the Government of Bangadesh, UWE-Augtex partnership PhD award, and UKRI Research England The Expanding Excellence in England (E3) grant. This work was submitted as a part of Sirui Tan's PhD thesis at the University of Manchester.

Conflict of Interest

The authors declare no conflict of interest.

Data Availability Statement

The data that support the findings of this study are available from the corresponding author upon reasonable request.

Keywords

bio-signal sensing, e-textiles, graphene, piezoresistive sensors, wearables

Received: July 29, 2022
Revised: September 23, 2022
Published online:

[1] L. Manjakkal, L. Yin, A. Nathan, J. Wang, R. Dahiya, *Adv. Mater.* **2021**, *33*, 2100899.
[2] M. Lin, Z. Zheng, L. Yang, M. Luo, L. Fu, B. Lin, C. Xu, *Adv. Mater.* **2022**, *34*, 2107309.
[3] B. Peng, F. Zhao, J. Ping, Y. Ying, *Small* **2020**, *16*, 2002681.
[4] R. He, H. Liu, Y. Niu, H. Zhang, G. M. Genin, F. Xu, *npj Flexible Electron.* **2022**, *6*, 20.
[5] Y. Lee, J. Kim, H. Joo, M. S. Raj, R. Ghaffari, D.-H. Kim, *Adv. Mater. Technol.* **2017**, *2*, 1700053.
[6] D. R. Seshadri, R. T. Li, J. E. Voos, J. R. Rowbottom, C. M. Alfes, C. A. Zorman, C. K. Drummond, *NPJ Digit Med* **2019**, *2*, 72.
[7] S. Chen, J. Qi, S. Fan, Z. Qiao, J. C. Yeo, C. T. Lim, *Adv. Healthcare Mater.* **2021**, *10*, 2100116.
[8] S. Lam Po Tang, *Transactions of the Institute of Measurement and Control* **2007**, *29*, 283.
[9] M. Stoppa, A. Chiolerio, *Sensors (Basel)* **2014**, *14*, 11957.
[10] M. R. Islam, S. Afroj, K. S. Novoselov, N. Karim, *Adv. Sci.* **2022**, 2203856.
[11] S. Afroj, M. H. Islam, N. Karim, *Proceedings* **2021**, *68*, 11.
[12] M. M. Hasan, M. M. Hossain, *J. Mater. Sci.* **2021**, *56*, 14900.
[13] Y. Wu, S. S. Mechael, T. B. Carmichael, *Acc. Chem. Res.* **2021**, *54*, 4051.
[14] N. Karim, S. Afroj, K. Lloyd, L. C. Oaten, D. V. Andreeva, C. Carr, A. D. Farmery, I.-D. Kim, K. S. Novoselov, *ACS Nano* **2020**, *14*, 12313.
[15] S. Afroj, N. Karim, Z. Wang, S. Tan, P. He, M. Holwill, D. Ghazaryan, A. Fernando, K. S. Novoselov, *ACS Nano* **2019**, *13*, 3847.
[16] N. Karim, S. Afroj, A. Malandraki, S. Butterworth, C. Beach, M. Rigout, K. S. Novoselov, A. J. Casson, S. G. Yeates, *J. Mater. Chem. C* **2017**, *5*, 11640.
[17] J. Zhu, C. Zhou, M. Zhang, *Soft Science* **2021**, *1*, 3.
[18] J.-w. Zhang, Y. Zhang, Y.-y. Li, P. Wang, *Polymer Reviews* **2021**, *62*, 65.
[19] J. Li, T. Wu, H. Jiang, Y. Chen, Q. Yang, *Advanced Intelligent Systems* **2021**, *3*, 2100070.
[20] H. Jung, D.-G. Gweon, *Rev. Sci. Instrum.* **2000**, *71*, 1896.
[21] X. Zeng, H.-T. Deng, D.-L. Wen, Y.-Y. Li, L. Xu, X.-S. Zhang, *Micromachines* **2022**, *13*, 254.
[22] J. Qin, L.-J. Yin, Y.-N. Hao, S.-L. Zhong, D.-L. Zhang, K. Bi, Y.-X. Zhang, Y. Zhao, Z.-M. Dang, *Adv. Mater.* **2021**, *33*, 2008267.
[23] J. Li, L. Fang, B. Sun, X. Li, S. H. Kang, *J. Electrochem. Soc.* **2020**, *167*, 037561.
[24] Q. Du, L. Liu, R. Tang, J. Ai, Z. Wang, Q. Fu, C. Li, Y. Chen, X. Feng, *Adv. Mater. Technol.* **2021**, *6*, 2100122.
[25] S. Maiti, M. R. Islam, M. A. Uddin, S. Afroj, S. J. Eichhorn, N. Karim, *Adv. Sustainable Syst.* **2022**, 2200258.
[26] M. H. Islam, M. R. Islam, M. Dulal, S. Afroj, N. Karim, *iScience* **2021**, 103597.
[27] N. Karim, S. Afroj, S. Tan, K. S. Novoselov, S. G. Yeates, *Sci. Rep.* **2019**, *9*, 1.
[28] M. H. Islam, S. Afroj, M. A. Uddin, D. V. Andreeva, K. S. Novoselov, N. Karim, *Adv. Funct. Mater.* **2022**, n/a, 2205723.
[29] S. Afroj, L. Britnell, T. Hasan, D. V. Andreeva, K. S. Novoselov, N. Karim, *Adv. Funct. Mater.* **2021**, *31*, 2107407.
[30] M. Marzana, M. M. A. Khan, A. Ahmed, M. A. Jalil, M. M. Hossain, in *Nanomaterials for Biocatalysis* (Eds: G. R. Castro, A. K. Nadda, T. A. Nguyen, X. Qi, G. Yasin), Elsevier, New York **2022**.
[31] N. Karim, S. Afroj, D. Leech, A. M. Abdelkader, in *Oxide Electronics* (Ed: A. Ray), John Wiley & Sons, Ltd, Hoboken, New Jersey **2021**, 2.
[32] N. Karim, S. Afroj, S. Tan, P. He, A. Fernando, C. Carr, K. S. Novoselov, *ACS Nano* **2017**, *11*, 12266.
[33] A. M. Abdelkader, N. Karim, C. Vallés, S. Afroj, K. S. Novoselov, S. G. Yeates, *2D Mater.* **2017**, *4*, 035016.
[34] R. Nolden, K. Zöll, A. Schwarz-Pfeiffer, *Materials (Basel)* **2021**, *14*, 2633.
[35] R. Seager, S. Zhang, A. Chauraya, W. Whittow, Y. Vardaxoglou, T. Acti, T. Dias, *IET Microwaves, Antennas & Propagation* **2013**, *7*, 1174.
[36] S. Qureshi, G. M. Stojanović, M. Simić, V. Jeoti, N. Lashari, F. Sher, *Materials (Basel)* **2021**, *14*, 7813.
[37] M. Martinez-Estrada, B. Moradi, R. Fernández-Garcia, I. Gil, *Sensors (Basel)* **2018**, *18*, 3824.
[38] M. Martínez-Estrada, B. Moradi, R. Fernández-Garcia, I. Gil, *Sensors (Basel)* **2019**, *19*, 1004.
[39] D. Bonefačić, J. Bartolić, *Sensors (Basel)* **2021**, *21*, 3988.
[40] J. Ren, C. Wang, X. Zhang, T. Carey, K. Chen, Y. Yin, F. Torrisi, *Carbon* **2017**, *111*, 622.
[41] M. R. Islam, S. Afroj, C. Beach, M. H. Islam, C. Parraman, A. Abdelkader, A. J. Casson, K. S. Novoselov, N. Karim, *iScience* **2022**, *25*, 103945.
[42] S. Afroj, S. Tan, A. M. Abdelkader, K. S. Novoselov, N. Karim, *Adv. Funct. Mater.* **2020**, *30*, 2000293.
[43] J. P. Rourke, P. A. Pandey, J. J. Moore, M. Bates, I. A. Kinloch, R. J. Young, N. R. Wilson, *Angew. Chem., Int. Ed.* **2011**, *50*, 3173.